Draft version May 8, 2006
Preprint typeset using LaTeX style emulateapj v. 6/22/04

THE VIPS VLA MINI-SURVEY

Kathleen F. Shurkin, Steven E. Tremblay, and George H. Heald
University of New Mexico, Department of Physics and Astronomy, 800 Yale Boulevard NE, Albuquerque, NM 87131
Draft version May 8, 2006

ABSTRACT

We present Very Large Array (VLA) and Very Long Baseline Array (VLBA) observations of a subsample of active galactic nuclei (AGN) in the "VLA Mini-Survey," which is itself a subsample of the VLBA Imaging Polarimetry Survey (VIPS). The VLA observations were obtained in continuum mode at 4.9 GHz, 8.5 GHz, and 14.9 GHz; the VLBA observations were obtained at 4.9 GHz. An analysis of the sources revealed 3 are resolved in the VLA and 5 are resolved in the VLBA. From the VLA observations, 5 are polarized in C, 9 are polarized in X, and 6 are polarized in U. A CSO candidate was found: J17309+3811.
Subject headings: galaxies:active—galaxies:jets—galaxies:surveys

1. INTRODUCTION

The VLBA Imaging and Polarization Survey (VIPS) consists of 1169 sources, all of which are active galactic nuclei (AGN), observed with the VLBA at 5 GHz with full polarization (see Taylor et al. 2005, ApJS, 159, 27 for a description of a pilot study). Some general goals of this survey are to gain a better understanding of AGN, as well as to find other sources of interest.

AGN are galaxies that exhibit intense, violent activity in their cores. They are incredibly bright, with luminosities in the range of 10^{43} to 10^{48} ergs s^{-1}. They are also very distant, with redshifts in the range 0.06 to 6.4. There are different types of AGN (quasars, blazars, radio galaxies, etc.), the distinction among them being dependent upon the angle of inclination of the host galaxy with respect to the line of sight. The generally accepted model is that AGN are powered by mass accretion onto supermassive black holes. This process accounts for the tremendous energy output, as the conversion of mass into energy in this manner is incredibly efficient (50% mass energy converted), even more so than nuclear fusion. As time progresses, the black hole devours the surrounding matter available for accretion and hence becomes dimmer. It follows that, when the black hole completely depletes its fuel supply, it becomes quiescent. Hence, AGN can provide clues as to the evolution of galaxies, as it is believed that many galaxies that posses supermassive black holes are now quiescent due to lack of fuel for the black holes in their cores. In addition, because they are so luminous and distant, they can also provide clues as to the evolution of the Universe in that they can be used as tools for probing much earlier epochs in the history of the Universe.

Despite the wealth of information about AGN, many questions remain as to the physical characteristics and processes behind many aspects of the central region, such as the formation and fueling of the black hole, the geometry of the central region itself, the production of jets, and emission mechanisms. This is where VIPS becomes important. VIPS is a survey that uses the VLBA, which, due to the long baselines, is capable of sufficient angular resolution to resolve parsec scale structure. VIPS will also provide polarization information about the sources. Magnetic fields, which are thought to be instrumental in the collimation of jets, can be determined from the observations of the linear polarization of the radio continuum emission. Also, because of the large sample size, the survey will provide a good representation of each different type of AGN. Of particular interest is a class of AGN called compact symmetric objects, or CSO, which are believed to be young radio galaxies.

In the "VLA Mini-Survey," we reduced, imaged, and analyzed data from observations of 10 VIPS sources. These sources are listed in Table 1, along with their positions and redshifts retrieved from NED.

TABLE 1
VIPS VLA Mini-Survey Sources

Source ID	R.A. (J2000.0)	Decl. (J2000.0)	Redshift (z) (NED, if available)
J16342+3203	16 34 12.79	32 03 35.4	2.34422
J16357+3629	16 35 47.24	36 29 30.0	—
J16474+3752	16 47 25.75	37 52 18.0	—
J16516+3528	16 51 39.82	35 28 40.5	—
J16498+3258	16 49 52.92	32 58 15.2	0.710851
J16534+3107	16 53 29.91	31 07 56.9	1.29839
1735+362 (A)	17 35 48.09	36 16 45.6	0.803
J17309+3811	17 30 54.11	38 11 50.9	—
J17289+3838	17 28 59.14	38 38 26.5	1.39
J17265+3957	17 26 32.67	39 57 02.2	0.66

2. OBSERVATIONS AND DATA REDUCTION

2.1. *VLA Observations*

Multi-frequency VLA observations of our sources were obtained on 2006 February 12 to yield information about the spectral indices or our sources. A total of 23 antennas were active (in A configuration) during the observing run (4 were out for the EVLA upgrade). Data were received in both left circular and right circular polarizations, and acquired through two 50 MHz bands yielding 100 MHz total bandwidth. The data were correlated with the NRAO's VLA correlator in NM. Observations were made in continuum mode with a central frequencies of 4860 MHz, 8460 MHz, and 14940 MHz. Antenna phases were established using phase referencing, with the two sources 1602+334 and 1735+362 as our references. The absolute flux was determined from observations of the

bright source 3C386. Time on source (see Table 2) varied, with a minimum of 37 seconds and a maximum of 167 seconds (the maximum occurs for a calibrator which had four separate observation intervals).

The data were reduced in AIPS, using the following tasks. QUACK and TVFLG were used to trim out bad data points, which were either due to slewing or high noise. The amount of flux for the primary calibrator, 3C286, was then set using SETJY and modeling it as a point source. CALIB was then used to correct the phase errors in the data, as well as amplitudes and the information was written into an SN table. The gains of the phase calibrator were then set using the task GETJY. CLCAL then merged the existing CL table with the SN table, creating an new CL table. The polarization cross- over was then corrected for by running PCAL with our unpolarized source, 1407+284. At this point, there still was an offset in the polarization angles that was determined by running RLDIF on 3C286, which has a known polarization angle. The angles were corrected using CLCOR. The task SPLIT was then used to make individual files for each of the sources at each frequency. Finally, FITTP was used to convert the split files to fits files.

Imaging of the sources was performed using DIFMAP. Initially, all of the sources were imaged using the CLEAN command, and further corrections in the data were made with SELFCAL if the signal to noise was appropriate for this procedure. None of the 14965 MHz data had SELFCAL performed on them because of the low flux and higher noise. Sources that showed extended emission were then modeled as Gaussian components using MODELFIT, from which the characteristics of the emission were determined.

2.2. *VLBA Observations*

Observations were obtained from NRAO's VLBA on 2006 January 03. A total of 9 antennas were active during the observing run (Owens Valley telescope wasn't operational during these observations). Data were received in both left circular and right circular polarizations, and acquired through four 8 MHz bands yielding 32 MHz total bandwidth. The data were correlated with the NRAO's VLBA correlator in Socorro, NM.

The data were reduced using AIPS before they were given to us.

Imaging of the sources was also performed using DIFMAP. Like the VLA data, these sources were imaged using the CLEAN command and further corrections in the data were made with SELFCAL. Sources which showed extended emission were then modeled as Gaussian components using MODELFIT, from which the characteristics of the emission were determined.

3. ANALYSIS

Of the 10 sources reduced and analyzed by our group, only 3 (J16474+3752, J17289+3838, J17265+3957) were resolved in the VLA observations, while 5 (J16534+3107, 1735+362, J17309+3811, J17289+3838, J17265+3957) were resolved in the VLBA observations. For each source, the location of the peak of the total intensity was measured in each band, and the flux in Stokes Q and U was extracted from the data at those locations. Using those values, the percent polarization was obtained by calculating

$$\sqrt{Q_{\rm max}^2 + U_{\rm max}^2}/I_{\rm max}, \quad (1)$$

and the polarization angle was obtained using

$$\frac{1}{2}\arctan\frac{U_{\rm max}}{Q_{\rm max}}. \quad (2)$$

Tables 3, 4, 5, and 6 show the peak flux density in each observation, as well as the derived percent polarization and polarization angles. The RMS noise was measured off source. Tables 7, 8, 9, and 10 show the RMS for each source in Stokes I, Q, and U.

The angular size of the jet, or the separation between resolved components if the source does not clearly show evidence of a jet, was obtained using modelfit components. The distance to the source was calculated using

$$d = \frac{c}{H_0}\frac{(z+1)^2-1}{(z+1)^2+1}, \quad (3)$$

the value for the Hubble constant H_0 being 75 km s^{-1} Mpc^{-1}. The actual linear separation between components or jet length was then calculated using

$$D = \frac{\alpha d}{206265}, \quad (4)$$

where D = linear size in parsecs, α = angular size in arcseconds, and d = distance in parsecs.

The lower limit of the core brightness temperature was calculated by using

$$T_b = \frac{c^2 S}{2k_B\nu^2\Omega} \quad (5)$$

and setting Ω = (beamwidth in radians)^2. Table 11 shows the lower limit on brightness temperature for each source.

3.1. *J16342+3203*

This source was not resolved in the VLA images. It has a steep spectral index of -0.51, suggesting that it could perhaps be a jet. This hypothesis is supported in that the radio image is off center in the optical image. The distance was calculated to be 3343.391 Mpc from the redshift (see Table 1). This source was found to be 1.60% polarized in C-band, 1.22% polarized in X-band, and 0.53% polarized in U-band. The VLBA recovered 93.3% of the VLA C-band flux.

3.2. *J16357+3629*

This source has a spectral index of -0.07. The fact that the spectrum is flat, along with the correspondence between the radio and optical images, suggests that this is a core. This source is 2.97% polarized in C-band, and 2.64% polarized in X-band. The VLBA recovered 92.9% of the VLA C-band flux.

3.3. *J16474+3752*

Since J16474+3752 is resolved out in the VLBA observation, we can assume that existing structure that is seen in the VLA images doesn't exist on the parsec scale. The spectral index for the center component was -1.0, and that of the other component was -1.6. The fact that these spectral indices are steep suggests that neither of them are core components. The separation between the components is 1.1 arcsec in C and X bands. The position angle in the VLA images is about 1° East of North. This source was found to be 6.3% polarized in C-band, 11.1% polarized in X-band, and 11.3% polarized in U-band.

3.4. *J16516+3528*

The spectral index of this source was calculated to be -0.33. The radio/optical overlay shows that there is no optical counterpart. This source was found to be 3.37% polarized in C-band, 4.14% polarized in X-band, and 4.50% polarized in U-band. The VLBA recovered 81.8% of the VLA C-band flux.

3.5. *J16498+3258*

This source was not resolved in the VLA. The spectral index peaks in X-band. The slope was taken between X-band and U-band, and is -0.14. This value, along with the fact that the radio image is at the center of the optical image, suggests that this could perhaps be a core. The distance was calculated to be 1962.827 Mpc from the redshift(see Table 1). This source was found to be 1.28% polarized in X-band, and 1.28% polarized in U-band. The VLBA recovered 89.9% of the VLA C-band flux.

3.6. *J16534+3107*

The VLBA image of J16534+3107 reveals parsec-level structure which is not present on the kiloparsec scale (VLA observations). The eastward jet is currently limited to being close to the core ($\sim$100 parsecs) which could suggest this is a young jet. Velocity measures from multi-epoch observations are needed to verify this hypothesis. The spectral index peaks in X-band. The slope was taken between X-band and U-band, and is -0.33. This value, along with the fact that the radio image is in the center of the optical image, suggests that the VLA image is dominated by a core component. The distance was calculated to be 2726.641 Mpc from the redshift(see Table 1). The position angle of the jet in the VLBA image is 96°. This source was found to be 1.32% polarized in X-band. The VLBA recovered 93.4% of the VLA C-band flux.

3.7. *1735+362*

This source was not observed with the VLA in C-band. It appears extended in the VLBA image. The radio image is slightly off center in the optical image. The spectral index was -0.24. The distance was calculated to be 2118.005 Mpc from the redshift (see Table 1). The VLBA jet has a position angle of 62.2° and a length of 9.5 mas, which corresponds to a linear length of 97.6 pc. This source was found to be 2.01% polarized in X-band and 2.09% polarized in U-band.

3.8. *J17309+3811*

The steep spectral index observed for J17309+3811 ($\alpha = -0.99$), along with the fact that both of the components visible in the VLBA image have comparable brightness suggest that J17309+3811 is a very good CSO candidate, and should be followed up on in particular. A redshift was not available for this source, so we could not calculate a distance. However, since there was no optical image of the source, it seems reasonable to expect that it is very distant. The separation between components in the VLBA image was 28.9 mas, with a position angle of PA 53.8°. This source was found to be 1.85% polarized in X-band and 1.43% polarized in U-band. The VLBA recovered 93.6% of the VLA C-band flux.

3.9. *J17289+3838*

This source has two components. The brighter component, which is at the center of the optical image, has a spectral index of -0.38, and the other component has a spectral index of -0.93. The spectral indices were determined using only C-band and X-band, as there was no sign of extension in the U-band image. The distance was calculated to be 2808.123 Mpc from the redshift (see Table 1). The VLA jet in C-band has a length of 1.57 arcsec, which correspondes to 21.3 kpc, and a position angle of 223.6°. The VLA jet in X-band has a length of 1.72 arcsec, which corresponds to 23.5 kpc, and a position angle of 224.9°. The VLBA jet has a length of 1.02 mas, which corresponds to 13.8 pc, and a position angle of $-106.6°$. The difference between the VLA and VLBA position angles is 63°. This source was not found to be polarized. The VLBA recovered 95.3% of the VLA C-band flux.

3.10. *J17265+3957*

This source has two bright components, one of which corresponds to the center of the optical image, and a dimmer, more complex extension to the Northwest in the VLA images. The extension in the VLBA image curves from Southwest to South. The spectral index of the center component was -0.47, and that of the other bright component was -0.94. The distance was calculated to be 1869.848 Mpc from the redshift (see Table 1). The VLA jet in C-band has a length of 0.87 arcsec, which corresponds to 7.9 kpc, and a position angle of 224.5°. The VLA jet in X-band has a length of 0.88 arcsec, which corresponds to 7.99 kpc, and a position angle of 224.6°. The VLA jet in U-band has a length of 0.89 arcsec, which corresponds to 8.07 kpc, and a position angle of 224°. The difference between the VLA and VLBA position angles is 40°. The VLBA jet has a length of 36.8 mas, which corresponds to 334 pc, and a position angle of 184.9°. This source was found to be 10.97% polarized in C-band, 10.7% polarized in X-band, and 5.39% polarized in U-band. The VLBA recovered 97% of the VLA C-band flux.

4. CONCLUSIONS AND FUTURE WORK

Of the 8 sources detected in VLBA and observed with the VLA at 4885 MHz, all recovered $\geq$ 80% of the flux, and 6 recovered $\geq$ 90% of the flux. See Figure 1.

Multi-frequency VLBA observations of sources that show parsec scale structure should be performed to get spectral indices from each individual component as well as rotation measures. Further observations at 5 GHz is also recommended so that evolution of the systems can be studied (e.g. velocities of components, changes in polarization, etc.). These sources should also be observed at other wavelengths (optical, infrared, etc.) to possibly learn about other properties of the host galaxies.

TABLE 2
VLA Times on Source (Seconds)

Source	C-band	X-band	U-band
J16342+3203	50	40	50
J16357+3629	37	40	48
J16474+3752	47	43	40
J16516+3528	40	40	40
J16498+3258	40	40	40
J16534+3107	40	40	40
1735+362	–[a]	90	167
J17309+3811	37	40	40
J17289+3838	50	50	40
J17265+3957	40	40	40

[a]Not observed in C-band.

TABLE 3
VLA C-band maximum flux density values, fractional polarization, and polarization angles

Source ID	Peak I (Jy beam^{-1})	Peak Q[a] (Jy beam^{-1})	Peak U[a] (Jy beam^{-1})	Fractional Polarization	Polarization Angle (°)
J16342+3203	0.19987	0.0015152	0.0028282	0.016053	30.91
J16357+3629	0.06757	-0.0018178	-0.00086288	0.02978	-77.304
J16474+3752	0.22769	-0.012552	-0.0071647	0.063476	-75.141
J16516+3528	0.075143	0.0025267	-0.00020035	0.033731	-2.2668
J16498+3258	0.077637	-0.00031805	-0.00057905	0.0085094	–
J16534+3107	0.47426	0.0026162	0.0021199	0.0071	–
1735+362[b]	–	–	–	–	–
J17309+3811	0.23341	-5.0655e-05	0.0002606	0.0011374	–
J17289+3838	0.22127	0.00020789	-6.8192e-07	0.00093954	–
J17265+3957	0.16419	-0.0086914	-0.015772	0.10968	-59.429

[a]Determined at spatial location of peak in total intensity (I) image
[b]Source 1735+362 not observed in C-band

TABLE 4
VLA X-band maximum flux density values, fractional polarization, and polarization angles

Source ID	Peak I (Jy beam^{-1})	Peak Q[a] (Jy beam^{-1})	Peak U[a] (Jy beam^{-1})	Fractional Polarization	Polarization Angle (°)
J16342+3203	0.16933	0.0020365	0.00031132	0.012167	4.3458
J16357+3629	0.065842	-0.00028717	-0.0017147	0.026405	-49.754
J16474+3752	0.13116	-0.014441	-0.0020831	0.11124	-85.896
J16516+3528	0.061709	0.0024793	0.00061501	0.041395	6.9657
J16498+3258	0.081099	-0.0004092	0.00095615	0.012824	56.585
J16534+3107	0.50031	0.00049622	0.0065845	0.013198	42.845
1735+362	0.55832	0.010976	0.0023588	0.020108	6.0643
J17309+3811	0.1384	-0.0020064	-0.0015803	0.018454	-70.887
J17289+3838	0.18872	-0.0001995	-0.00024251	0.001664	–
J17265+3957	0.12506	-0.010137	-0.0087097	0.10687	-69.665

[a]Determined at spatial location of peak in total intensity (I) image

TABLE 5
VLA U-band maximum flux density values, fractional polarization, and polarization angles

Source ID	Peak I (Jy beam^{-1})	Peak Q[a] (Jy beam^{-1})	Peak U[a] (Jy beam^{-1})	Fractional Polarization	Polarization Angle (°)
J16342+3203	0.11211	-0.00012654	0.00057758	0.0052741	–
J16357+3629	0.062395	5.6905e-05	-0.00017641	0.0029708	–
J16474+3752	0.064229	-0.0070873	0.0016803	0.1134	83.331
J16516+3528	0.052049	-4.7597e-05	0.0023439	0.045042	45.582
J16498+3258	0.075045	0.00094887	0.00015058	0.012802	4.5087
J16534+3107	0.41502	0.0032072	-0.00011204	0.0077325	–
1735+362	0.48838	0.010195	0.00015528	0.020878	0.4363
J17309+3811	0.077079	0.0010283	0.00040636	0.014345	10.781
J17289+3838	0.14404	-7.6656e-05	0.00042214	0.0029786	–
J17265+3957	0.094565	-0.0033984	-0.003793	0.053854	-65.93

[a]Determined at spatial location of peak in total intensity (I) image

TABLE 6
VLBA C-band maximum flux density values, fractional polarization, and polarization angles

Source ID	Peak I (Jy beam^{-1})	Peak Q[a] (Jy beam^{-1})	Peak U[a] (Jy beam^{-1})	Fractional Polarization	Polarization Angle (°)
J16342+3203	0.16649	0.011412	0.011018	0.095278	23.003
J16357+3629	0.058792	0.010335	0.010559	0.251312	22.193
J16474+3752	0.014398	0.010045	0.0099461	0.981804	22.642
J16516+3528	0.040969	0.011319	-0.00018058	0.276317	45.457
J16498+3258	0.065793	0.011424	0.010891	0.239898	23.184
J16534+3107	0.35876	0.010697	0.011093	0.042955	21.979
1735+362	0.42526	0.011806	0.012562	0.040538	21.612
J17309+3811	0.054194	0.010417	0.010175	0.268697	22.837
J17289+3838	0.18778	0.011405	0.010690	0.083245	23.427
J17265+3957	0.056509	0.010097	0.010801	0.261649	21.535

[a]Determined at spatial location of peak in total intensity (I) image

TABLE 7
VLA C-band RMS noise (milliJansky)

Source	Stokes I	Stokes Q	Stokes U
J16342+3203	0.2778	0.1987	0.2037
J16357+3629	0.2396	0.2344	0.3806
J16474+3752	0.2255	0.2408	0.2600
J16516+3528	0.2112	0.2316	0.2371
J16498+3258	0.2911	0.2894	0.3091
J16534+3107	0.2898	0.2523	0.2588
1735+362[a]	–	–	–
J17309+3811	0.2531	0.2537	0.2397
J17289+3838	0.2472	0.2259	0.2315
J17265+3957	0.2165	0.2302	0.2366

[a]Not observed in C-band.

TABLE 8
VLA X-band RMS noise (milliJansky)

Source	Stokes I	Stokes Q	Stokes U
J16342+3203	0.3098	0.1929	0.1851
J16357+3629	0.2004	0.2824	0.1711
J16474+3752	0.1868	0.1737	0.1874
J16516+3528	0.2259	0.2094	0.1963
J16498+3258	0.1718	0.1874	0.1809
J16534+3107	0.2906	0.1743	0.1820
1735+362	0.1297	0.1265	0.1336
J17309+3811	0.1847	0.1691	0.1898
J17289+3838	0.1869	0.1725	0.1806
J17265+3957	0.1701	0.1924	0.1743

TABLE 9
VLA U-band RMS noise (milliJansky)

Source	Stokes I	Stokes Q	Stokes U
J16342+3203	0.7312	0.4490	0.4211
J16357+3629	0.6576	0.7159	0.6044
J16474+3752	0.7918	0.7642	0.7590
J16516+3528	0.8470	0.7903	0.7900
J16498+3258	0.7988	0.7668	0.7960
J16534+3107	0.8902	0.7894	0.7902
1735+362	0.4062	0.426	0.3982
J17309+3811	0.8003	0.9012	0.7400
J17289+3838	0.7785	0.7859	0.7457
J17265+3957	0.8443	0.8476	0.8887

TABLE 10
VLBA C-band RMS noise (milliJanksy)

Source	Stokes I	Stokes Q	Stokes U
J16342+3203	0.2823	0.2951	0.2911
J16357+3629	0.3186	0.2890	0.2983
J16474+3752	0.3597	0.2804	0.2974
J16516+3528	0.3000	0.3019	0.3033
J16498+3258	0.3098	0.3076	0.2843
J16534+3107	0.2772	0.2877	0.2933
1735+362	0.2870	0.3021	0.2914
J17309+3811	0.2602	0.2579	0.3011
J17289+3838	0.2803	0.2713	0.2746
J17265+3957	0.2757	0.3095	0.4171

TABLE 11
Core Brightness Temperature (Kelvin)

Source	C-band	X-band	U-band
J16342+3203	72146.12[a]	56422.34[a]	35726.73[a]
J16357+3629	24390.42	21939.17	19883.77
J16474+3752	82188.17	43703.74	20468.22
J16516+3528	27124.01	20563.01	16586.75
J16498+3258	28024.26	27022.94	23915.01
J16534+3107	171191.4	166708 132256.8	
1735+362	–[b]	186037.4[a]	155634.8[a]
J17309+3811	84252.89[a]	46116.17[a]	24563.2[a]
J17289+3838	79870.77	62883.26	45902.04
J17265+3957	59266.88	41671.16	30135.56

[a]Source shows no apparent signs of a core component
[b]Not observed in C-band

TABLE 12
Comparison between VLA C-band and VLBA C-band

Source ID	VLA Peak (mJy/beam)	VLA PA (degrees)	VLA L (kpc)	VLBA Peak (mJy/beam)	VLBA S (mJy)	VLBA PA (degrees)	VLBA L (pc)	f ($S_{VLBA}/Peak_{VLA}$)	ΔPA (degrees)
J16342+3203	199.9	1	–	166.5	186.5	–	–	0.933	–
J16357+3629	67.57	–	–	58.79	62.77	–	–	0.929	–
J16474+3752	227.7	–	–	14.40	–	–	–	–[a]	–
J16516+3528	75.14	–	–	4.097	61.47	–	–	0.818	–
J16498+3258	77.63	–	–	6.579	69.80	–	–	0.899	–
J16534+3107	474.3	–	–	358.8	443.0	96	119	0.934	–
1735+362	–[b]	–	–	425.3	62.2	97.6	–[b]	–	–
J17309+3811	233.4	–	–	54.19	218.5	53.8	28.9 mas	0.936	–
J17289+3838	221.3	223.6	21.3	187.8	210.9	-106.6	13.8	0.953	117
J17265+3957	164.2	224.5	7.9	56.51	159.3	184.9	334	0.97	40

[a]Not detected with VLBA
[b]Not observed in C-band

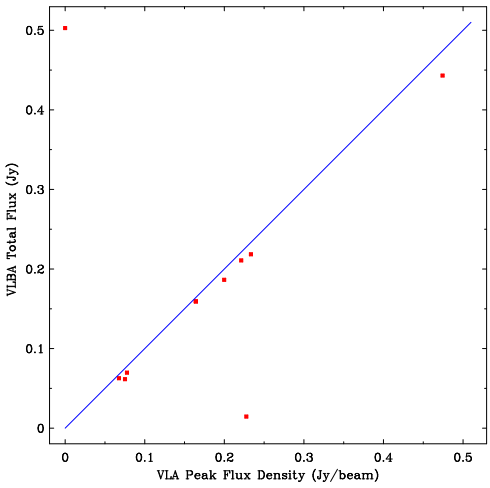

FIG. 1.— VLBA total flux vs. VLA peak flux density. Solid line shows ratio of unity.

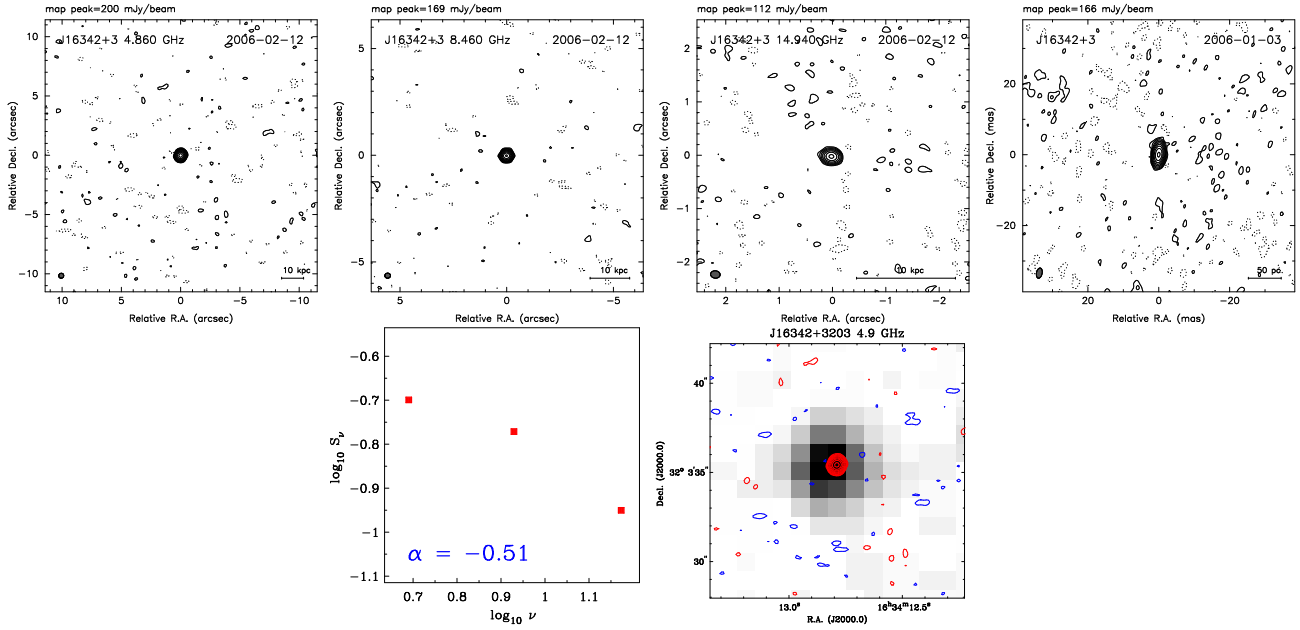

FIG. 2.— J16342+3203, top left to top right: VLA C-band, VLA X-band, VLA U-band, VLBA X-band; bottom left to bottom right: Spectral index plot, Radio-optical overlay (4.9 GHz VLA image with Digitized Sky Survey image)

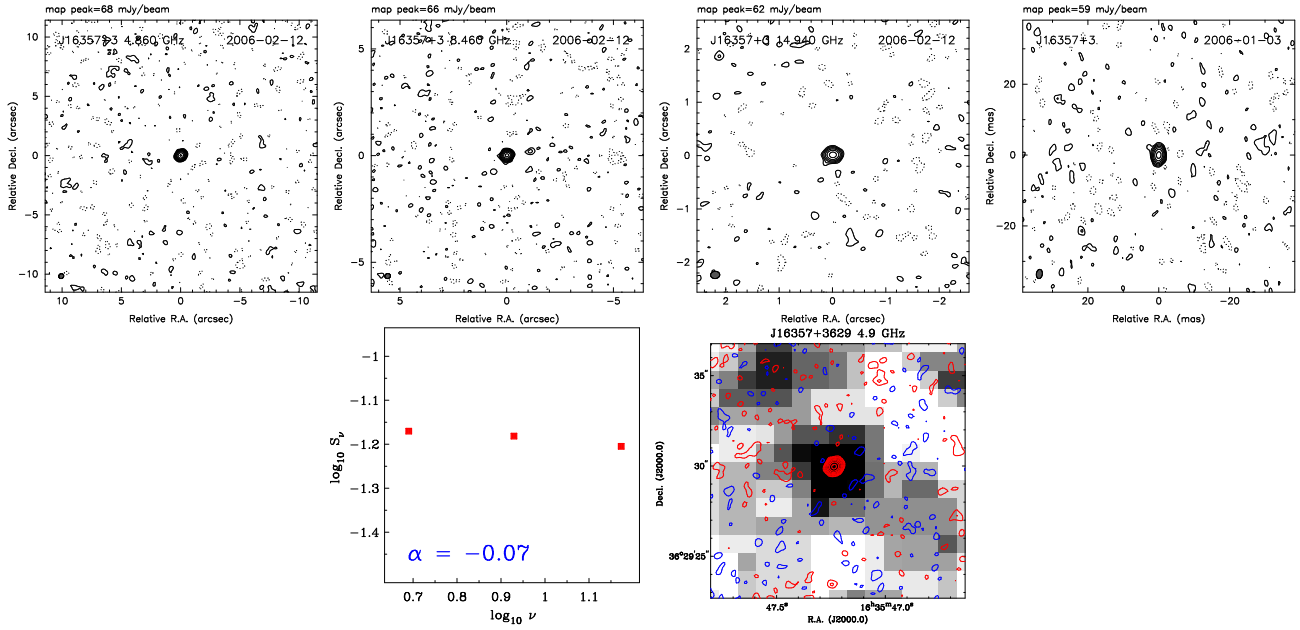

FIG. 3.— J16357+3629, top left to top right: VLA C-band, VLA X-band, VLA U-band, VLBA X-band; bottom left to bottom right: Spectral index plot, Radio-optical overlay (4.9 GHz VLA image with Digitized Sky Survey image)

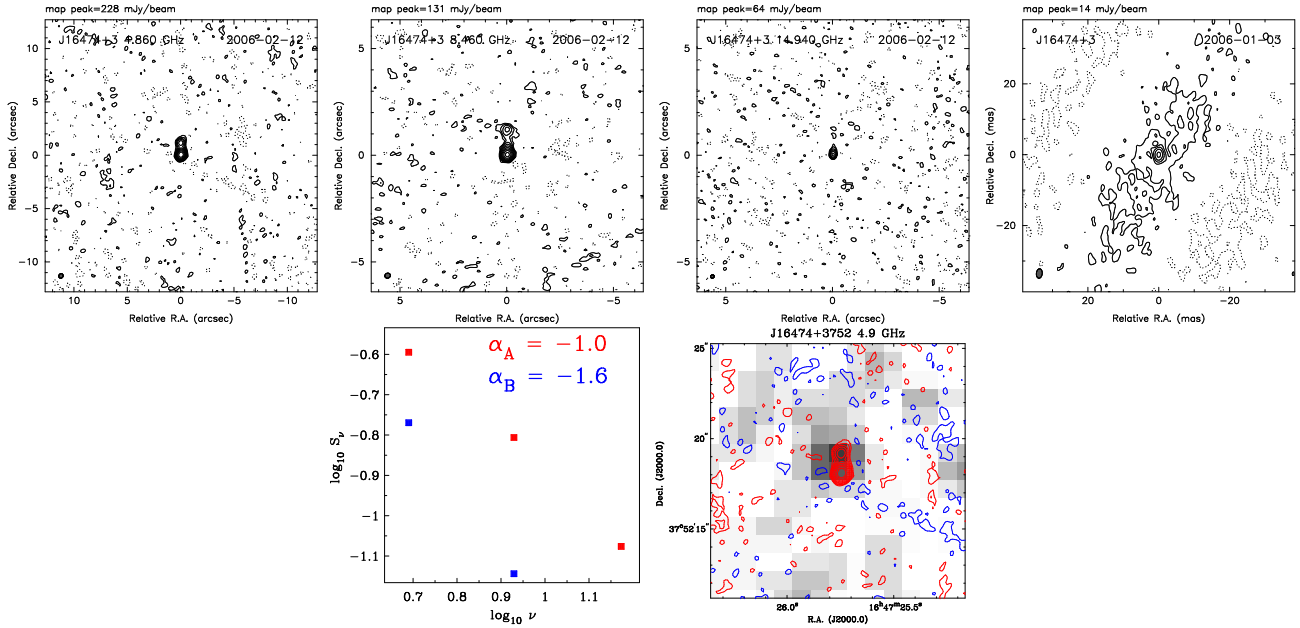

FIG. 4.— J16474+3752, top left to top right: VLA C-band, VLA X-band, VLA U-band, VLBA X-band (Non-detection); bottom left to bottom right: Spectral index plot, Radio-optical overlay

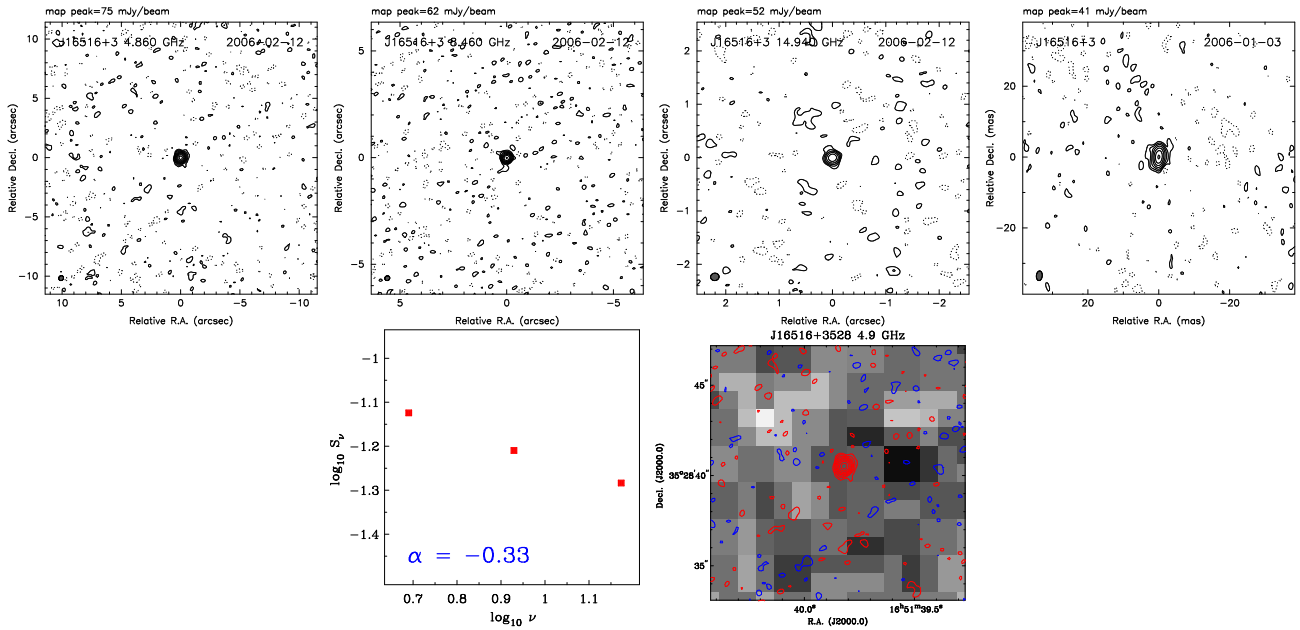

FIG. 5.— J16516+3528, top left to top right: VLA C-band, VLA X-band, VLA U-band, VLBA X-band; bottom left to bottom right: Spectral index plot, Radio-optical overlay (4.9 GHz VLA image with Digitized Sky Survey image)

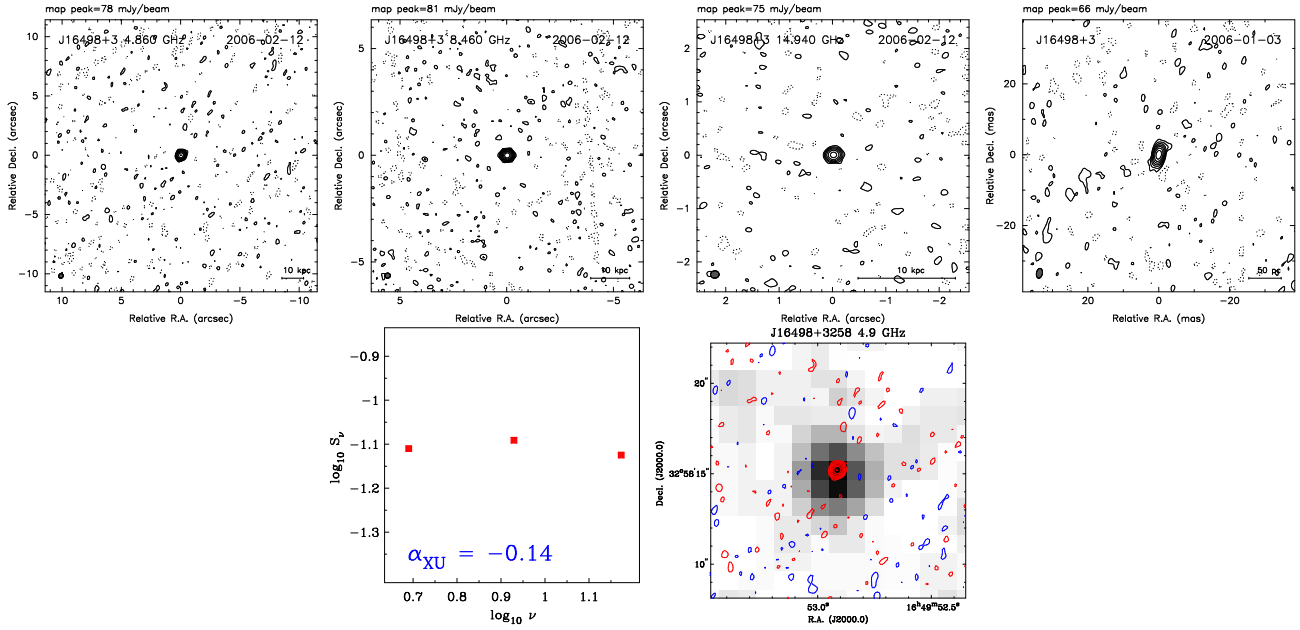

FIG. 6.— J16498+3258, top left to top right: VLA C-band, VLA X-band, VLA U-band, VLBA X-band; bottom left to bottom right: Spectral index plot, Radio-optical overlay (4.9 GHz VLA image with Digitized Sky Survey image)

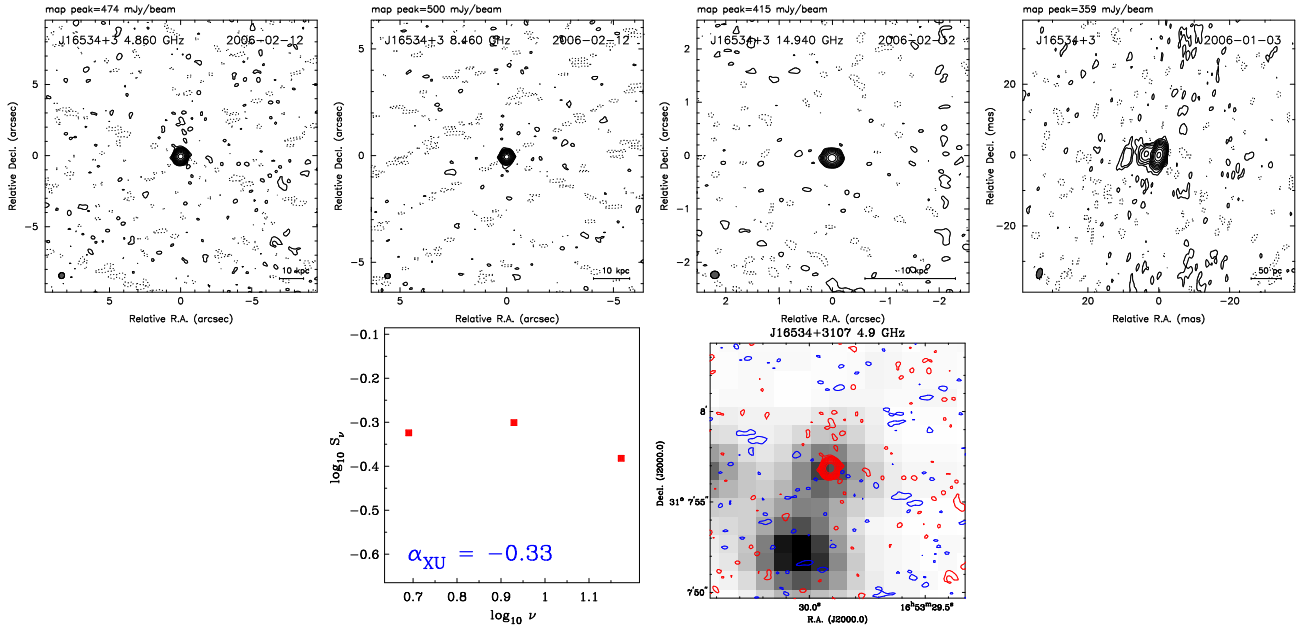

FIG. 7.— J16534+3107, top left to top right: VLA C-band, VLA X-band, VLA U-band, VLBA X-band; bottom left to bottom right: Spectral index plot, Radio-optical overlay (4.9 GHz VLA image with Digitized Sky Survey image)

Nothing to see here...

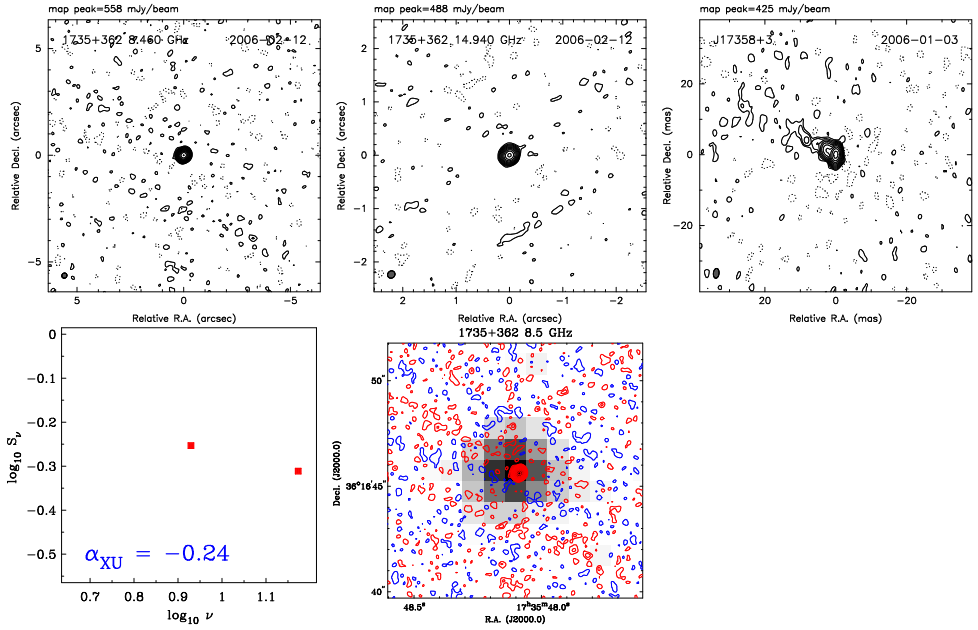

FIG. 8.— 1735+362, top left to top right: VLA C-band (not observed), VLA X-band, VLA U-band, VLBA X-band; bottom left to bottom right: Spectral index plot, Radio-optical overlay (8.5 GHz VLA image with Digitized Sky Survey image)

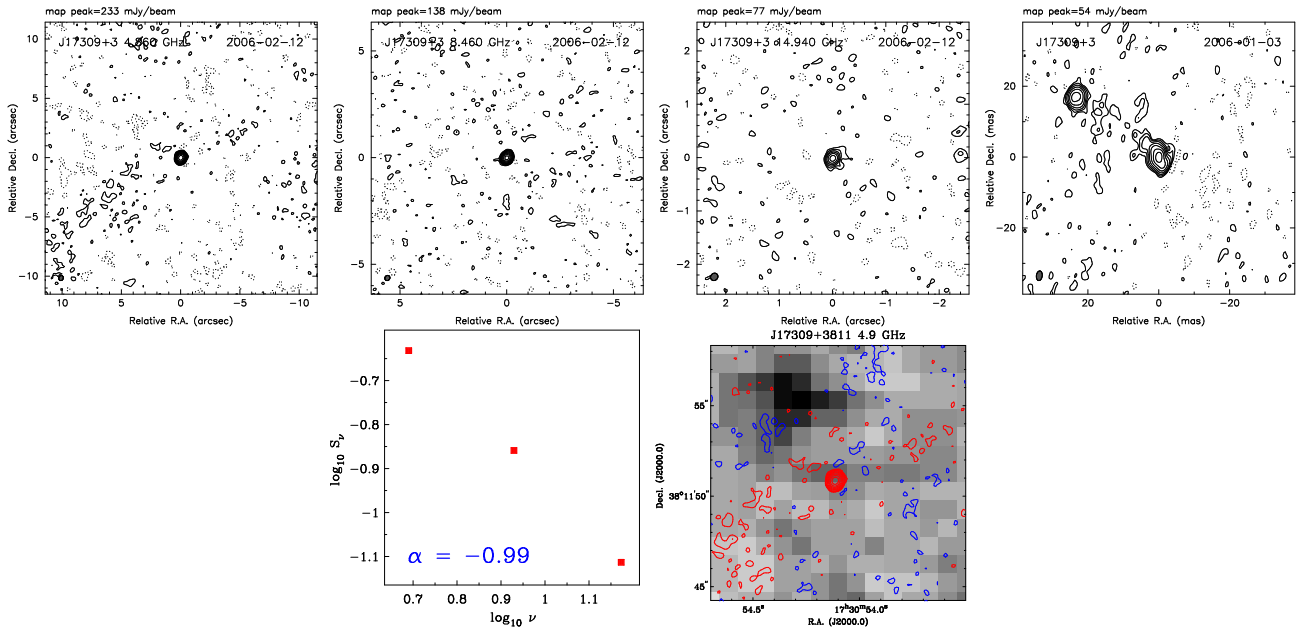

FIG. 9.— J17309+3811, top left to top right: VLA C-band, VLA X-band, VLA U-band, VLBA X-band; bottom left to bottom right: Spectral index plot, Radio-optical overlay (4.9 GHz VLA image with Digitized Sky Survey image)

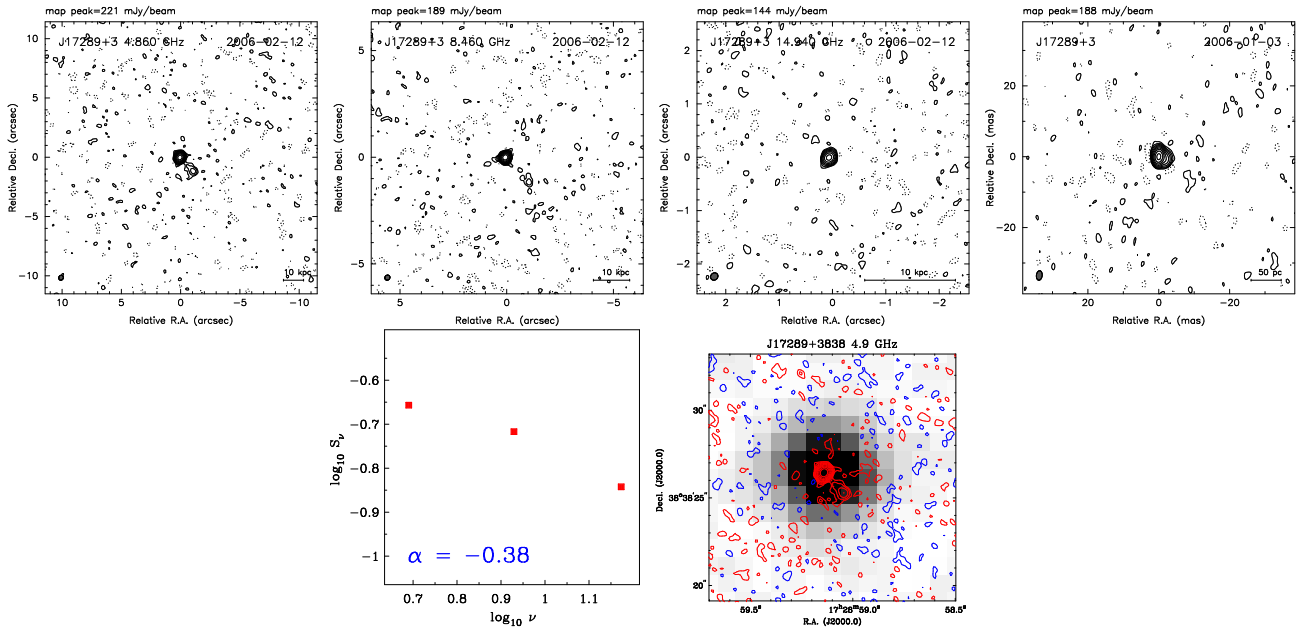

FIG. 10.— J17289+3838, top left to top right: VLA C-band, VLA X-band, VLA U-band, VLBA X-band; bottom left to bottom right: Spectral index plot, Radio-optical overlay (4.9 GHz VLA image with Digitized Sky Survey image)

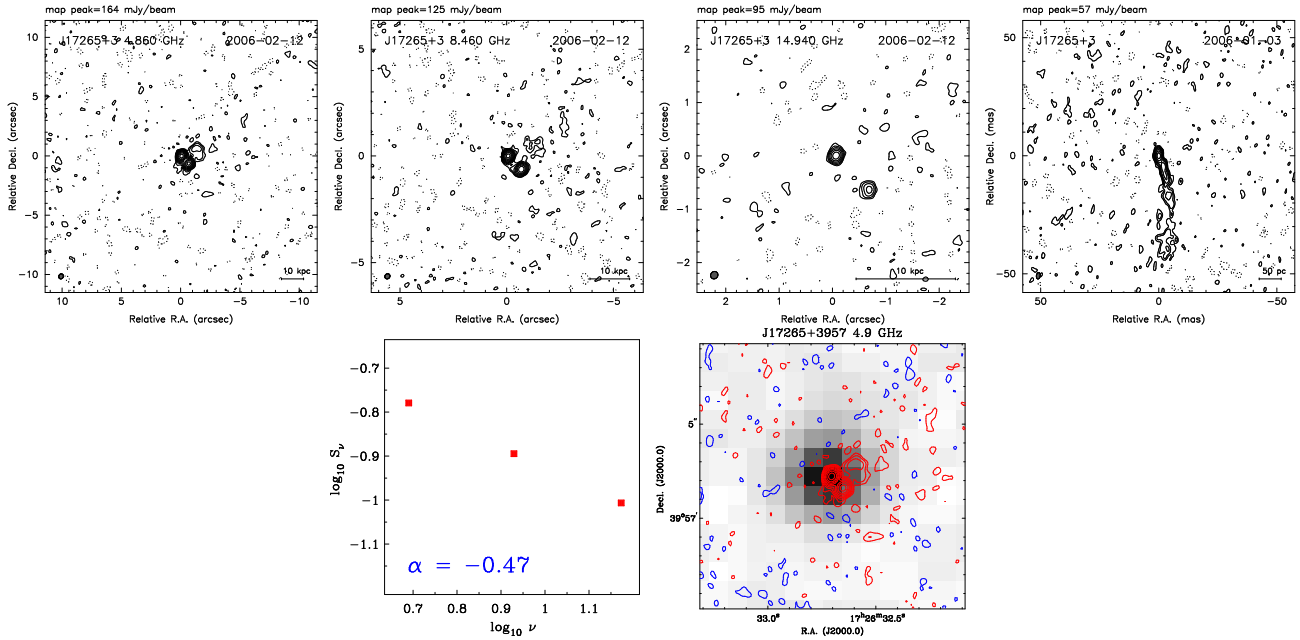

FIG. 11.— J17265+3957, top left to top right: VLA C-band, VLA X-band, VLA U-band, VLBA X-band; bottom left to bottom right: Spectral index plot, Radio-optical overlay (4.9 GHz VLA image with Digitized Sky Survey image)